The effect of hydrochloric acid on microstructure of porcine (Sus scrofa domesticus) cortical bone tissue

Sabolova, Veronika; Brinek, Adam; Sladek, Vladimir

Published in:
Forensic Science International

DOI:
10.1016/j.forsciint.2018.08.030

Publication date:
2018

Document Version
Peer reviewed version

Title: The effect of hydrochloric acid on microstructure of porcine Sus scrofa domesticus cortical bone tissue

Authors: Veronika Sabolová, Adam Brinek, Vladimír Sládek

PII: S0379-0738(18)30663-7
DOI: https://doi.org/10.1016/j.forsciint.2018.08.030
Reference: FSI 9454

To appear in: *FSI*

Received date: 3-5-2018
Revised date: 15-8-2018
Accepted date: 25-8-2018

Please cite this article as: Veronika Sabolová, Adam Brinek, Vladimír Sládek, The effect of hydrochloric acid on microstructure of porcine Sus scrofa domesticus cortical bone tissue, Forensic Science International https://doi.org/10.1016/j.forsciint.2018.08.030

The effect of hydrochloric acid on microstructure of porcine (*Sus scrofa domesticus*) cortical bone tissue

Veronika Sabolová*[1], Adam Brinek[2], Vladimír Sládek[1]

1 – Faculty of Science, Charles University, Viničná 7, 128 43 Prague 2, Czechia

2 – CEITEC – Central European Institute of Technology, Brno University of Technology

***Corresponding author: *E-mail address*: sabolova.veronika@gmail.com**

Graphical abstract

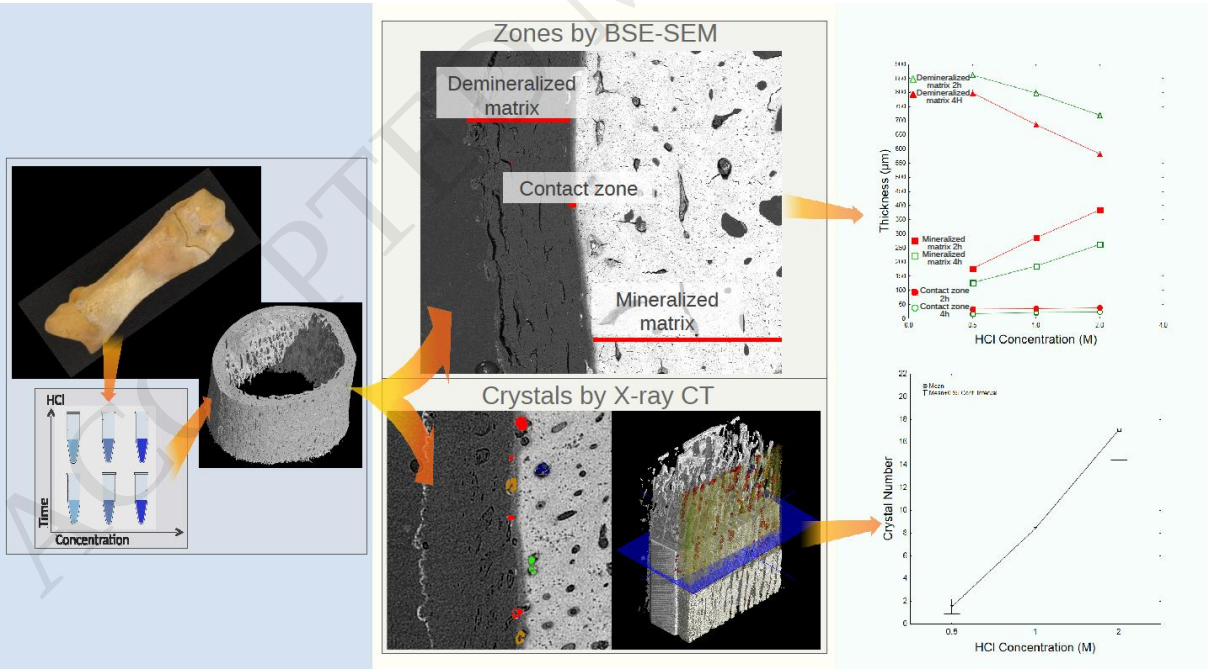

Highlights

- After immersion in HCl three zones appear in transversal section of cortical bone
- Observed zones vary according to HCl concentration and time of acid immersion
- HCl immersion has different effect on cortical bone according to anatomical location
- HCl immersion induced presence of crystals in Havers canals and periosteal boundary
- Presence of crystals suggests HCl demineralization also via lacuno-canalicular space

Abstract

We evaluated the degradation of cortical bone tissue by hydrochloric acid (HCl) since intentional bone decalcification in a forensic context has not been studied on a histomorphological level. We used 70 pig metatarsal bones split into subsamples and immersed in one of three concentrations of acidic solutions (0.5 M, 1 M, 2 M HCl) for two and four hours. We analyzed the cortical thicknesses on transversal cross-sections, thicknesses of the three histomorphologically distinct zones present in acid-immersed bones, and number and area of crystals present in one of the zones. Furthermore, we analyzed the ratio of calcium to phosphorus (Ca:P). We observed a division of the cortical bone cross section into three distinctive zones: demineralized matrix (DM) in the periosteal part of bone, middle contact zone (CZ), and mineralized matrix (MM) in the endosteal part of bone. With increasing acid concentration and time of immersion (from 0.5 M HCl for 2 h to 2 M HCl for 4 h), the thickness of DM increased by 67%, the thickness of CZ increased by 56%, and the thickness of MM decreased by 32%. The Ca:P ratio in the contact zone of acid-treated samples did not change significantly with changing acid concentration and time of immersion. The Ca:P ratio of the CZ decreased by 10% when

compared to the Ca:P ratio of MM in acid-treated samples. Moreover, we observed crystals on the outer periosteal border of the DM zone, in the CZ, and in the MM Haversian/Volkmann's canals. The size and number of the crystals in the CZ of acid-treated bones increased with acid concentration and time of acid immersion. Moreover, we also observed significant differences in all analyzed properties between anatomical regions. Due to varying reactions to acid immersion among anatomical regions, bone micro-degradation should be observed separately for each region.

KeyWords: hydrochloric acid, taphonomy, SEM, EDX, micro CT

Introduction

Post-mortem bone alterations caused by changing pH can be part of both pre- and post-burial processes and can be caused by human intervention as well as the natural environment surrounding deposited bone (Turner-Walker, 2007; López-Costas et al., 2016; Schotsmans and de Voorde, 2017). Acids (pH < 7) cause corrosive changes in bones (Cope and Dupras, 2009; Hartnett et al., 2011). Macroscopically, acid-caused bone degradation is characterized by loss of tissue and surface etching and cracking (Fernández-Jalvo and Andrews, 2016). Hartnett et al. (2011) describe the dissolution of bone in hydrochloric acid with stages of pitting and edge erosion through gradual softening of the tissue, turning it into a gelatinous and amorphous material. Microscopic bone changes caused by hydrochloric acid involve increased porosity and micro-cracking, and the bone mineral composition is depleted of calcium, phosphorus, and magnesium (Fernández-Jalvo and Andrews, 2016). Lee-Thorp and van der Merwe (1991) report chemical changes in bone experimentally immersed in acetic acid, where hydroxyapatite is

recrystallized into brushite. Furthermore, Lewandrowski et al. (1997) and Horneman et al. (2004) describe two zones observed in bone cross section after hydrochloric acid treatment, i.e., periosteal demineralized matrix followed by mineralized matrix in the endosteal part. Lewandrowski et al. (1997) also mention an interface at the reaction front between the demineralized and non-demineralized portion of the bone with a thickness of 20 µm, although no further morphologic description of the interface is given in their study. There is also a lack of description of acid-induced microscopic changes to fresh bone in terms of its histological morphology and of the progress of hydrochloric acid through the cortical bone tissue, which could be relevant in forensic investigations where bones are found and acid exposure is suspected.

Bone degradation by an acidic environment starts immediately after death when the decreasing amount of oxygen in the blood and build-up of various metabolites in the body decrease the pH of the body (Donaldson and Lamont, 2013). The micro-balance and structural support between the organic (mostly collagen) and inorganic (mostly hydroxyapatite) parts of the bone collapses and, also due to endogenous bacteria consuming the organic part, the bone begins to degrade (White and Booth, 2014). The degradation can be further accelerated by the environment in which the bone is deposited, and the disruption of the inorganic part progresses as the bone attempts to achieve a new state of chemical and physical equilibrium with the surrounding environment (Hedges, 2002; King et al., 2011). Naturally occurring environments with acidic pH include acidic soils (Nicholson, 1996), acidic aquatic environments (Hedges and Millard, 1995; Christensen and Myers, 2011), and environments with bacterial, fungal and invertebrate activity (Child et al., 1993; Nicholson, 1996; Hopkins et al., 2000; Jans et al., 2004;

Higgs et al., 2011). Another specific case of natural acidic bone degradation is that in which bones are partially digested by scavengers (Denys, 2002).

The anthropogenic bone exposures to acids are attempts to dispose of evidence of crime by dissolving it in specific corrosive substances (Cope and Dupras, 2009; Hartnett et al., 2011; Schotsmans and de Voorde, 2017). Existing research describes qualitative and quantitative (mostly weight) macroscopic changes to human bone, teeth, nails, and hair caused by corrosive agents such as hydrochloric, nitric, sulfuric, and phosphoric acid, with hydrochloric acid being the most detrimental (Mazza et al., 2005; Cope and Dupras, 2009; Hartnett et al., 2011). There is, however, a lack of quantification of microscopic changes to bone tissue caused by hydrochloric acid. Furthermore, 3D analysis of bone changes after its immersion in hydrochloric acid has also not been reported.

Another case of intentional anthropogenic bone alteration is that of decalcification protocols (Walsh and Christiansen, 1995; Zhang et al., 1997). Decalcification by hydrochloric acid is used in histology, medicine, and biomaterial research where the tissue is demineralized as only the organic element of bone is of interest (Castro-Ceseña et al., 2011; Figueiredo et al., 2011; El-Bassyouni et al., 2013). The progress of bone decalcification is quantified on a micro scale; however, there is a lack of information on complex histomorphologic bone changes in the context of biochemical and material research.

As the influence of the environment on degrading bone is very complex, field-based taphonomic experiments aim to recreate the events of degradation with the same complexity (Nicholson, 1996; Nielsen-Marsh and Hedges, 2000; Collins et al., 2002; Fernández-Jalvo et al., 2010; Hollund et al., 2013). There are also studies observing the effect of one isolated factor on the degradation of bodies outside of field or real-life scenarios. For example, Mazza et al. (2005)

dissolved isolated teeth in various acids to address the question of whether it is possible to destroy a cadaver by acid immersion. The study of Mazza et al. (2005) is an example where laboratory-based experiments fill in the information gap despite the loss of field context.

The goal of this paper is to describe the effect of hydrochloric acid degradation of cortical bone transversal cross sections on a histomorphological level. Further, we aim to quantify changes in cortical bone thickness, calcium and phosphorus ratio, and crystals within the contact zone, studying the effect of acid concentration and time of immersion. By using scanning electron microscopy (SEM) with energy dispersive X-ray spectroscopy (EDX), we aim to evaluate the dependency of the progress of the acid through the bone tissue on bone histomorphology. With the application of micro computed tomography, we aim to visualize the spatial arrangement and details of crystals within the contact zone. The final goal is to find possible histomorphological indicators of hydrochloric acid exposure that are potentially useful in forensic investigations.

Materials and Methods

Sample

The total sample consists of 70 right porcine (*Sus scrofa domesticus*) third metatarsal bones. The animals were raised in the Czech Republic (PIC genetics, mother line of Camborough breed and father line of PIC 408/337 breed). The age for slaughtering of pigs at this slaughterhouse was between 150 and 160 days, when the pigs reached the weight of approximately 118 kg. The bones were dissected out from fresh pig feet purchased from a slaughterhouse the day after the animals were slaughtered. The mean maximum length and its SD of bones used in the experiment was 82.6 ± 3.42 mm.

Histological section preparation

The total sample was divided into six subsamples treated in acid and one control subsample. Each subsample contained ten bones. After a bone was dissected out, the periosteum was carefully removed, and the maximum bone length was measured on an osteometric board. The bones were then immersed in separate glass bottles containing 200 ml of hydrochloric acid. Acid-treated subsamples were immersed in one of three acid solutions (0.5 M, 1 M, and 2 M HCl) for two and four hours. The bone was not exposed to agitation while immersed in acid. After the immersion, the bone was washed under running water for 5 minutes and subsequently cut at 50% of its maximal length with a handsaw. A cross-sectional slice (10 mm thick) was then cut away from the distal half of each bone using a Buehler IsoMet 1000 precision saw. The bone marrow was removed, and the cortical bone samples were then fixed in solution prepared according to Karnovsky (1965) and dehydrated in ethanol solutions with increasing concentrations (70%, 80%, 90%, and 100%) (Goldschlager et al., 2010). The fixed and dehydrated cuts were subsequently embedded in Epofix (EMS), polished, and carbon-coated.

SEM and EDX analysis

The physical changes observed in acid-treated bones were quantified by measuring the total cortical bone thickness and the thickness of histomorphologically distinct zones observed within the cortical bone of acid-treated bones. The histomorphologically distinct zones were named according to observed morphological properties which cortical bone acquired after the acid exposure (detailed description of histomorphological observations are included in the results section). The observed histomorphologically distinct zones were demineralized matrix (DM), contact zone (CZ), and mineralized matrix (MM) (Figure 1). Total cortical thickness and the thickness of the histomorphologically distinct zones were measured from the images of transversal cortical cross sections using the software Fiji (Schindelin et al., 2012). The images

were obtained using the backscattered electron mode of the scanning electron microscope (BSE-SEM) (TESCAN Vega, Czech Republic). The whole cross sections were scanned with a resolution of 1024 × 1024 pixels and magnification of 15×. The images of whole cross-sections were then digitalized using EPJ macro in Fiji (Sládek et al., 2018). The result of digitalization were axes in maximum and minimum second moments of area (I_{max} and I_{min}), defined as maximum and minimum principal axes across which the bone rigidities are greatest and least, respectively (Ruff, 2008). The I_{max}/I_{min} axes are biomechanical cross-sectional geometric properties of bone, which are not the subject of the current study. However, they were used to standardize the locations for measurement of cortical bone thickness as it has been proven that histological bone structure corresponds with bone loading (Jindrová et al., 2016). Four anatomical regions (anterior, posterior, medial, and lateral) were defined on each cross-section using I_{max} and I_{min} (Figure 2). The anatomical regions were scanned at a resolution of 1280 × 1280 pixels and a magnification of 62×. After the microscope scanning, the total cortical thickness and thicknesses of the histomorphologically distinct zones observed within the cortical bone of acid-treated bones were measured along the I_{max}/I_{min} axes from the four images of the anatomical regions.

The chemical changes were quantified by measuring and comparing the calcium and phosphorus ratios (Ca:P). The Ca:P values were obtained using an energy dispersive X-ray spectroscopy (EDX) detector (X-Max 50, Oxford Instruments, United Kingdom) after the SEM scanning. In controls, the spectroscopic values were taken from the periosteal, mid-cortical, and endosteal parts of the cortical bone. In the case of the acid-treated samples, the spectroscopic values were taken from the middle of the three zones present in the cross sections.

Crystal structures in the contact zone were identified and analyzed from the SEM images of acid-treated bones using the Fiji software. Crystals present in the contact zone were characterized by their number and area per mm^2 of contact zone.

Micro CT analysis

Numbers and volumes of crystals in the contact zone were also analyzed from the micro CT scan. One resin-embedded acid-treated sample (1 M/2 h) was cut in the medial anatomical region. A subsample with a size of 2 × 2 × 5 mm was scanned with a 500 ms exposure time, 70 kV acceleration voltage, X-ray tube current of 130 µA and a 1 mm aluminum filter. The achieved linear voxel size was 2 µm. The crystals were segmented from the images, and their counts and volumes were calculated using software VG Studio MAX 3.1 (Volume Graphics GmbH, Germany).

The micro CT scanning was performed using the GE Phoenix v|tome|x L 240 laboratory system (GE Sensing & Inspection Technologies GmbH, Germany) equipped with a nanofocus X-ray tube with 180 kV/15 W and high-contrast flat panel with 2048 px × 2048 px. The tomographic reconstruction was realized using the GE phoenix datos|x 2.0 software (GE Sensing & Inspection Technologies GmbH, Germany) with correction for sample drift and beam hardening.

Statistical analysis

All data are presented as the mean and standard deviation (SD). The effects of acid concentration and time of immersion on bone morphologic, chemical, and crystal changes were tested using one-way ANOVA. The differences were considered statistically significant if $p <$

0.05. All statistical analyses were performed using software STATISTICA 13.2 for Windows (StatSoft Inc., 2015).

Results

Morphological changes

Figure 1 shows histomorphology of the lateral anatomical region of bone cross section after treatment in 2 M hydrochloric acid for 4 h. Cortical bone changed in appearance and three distinctive zones were observed: demineralized matrix (DM), contact zone (CZ), and mineralized matrix (MM). The demineralized matrix is of dark gray color with a thickness of approximately 600 μm and was observed in the sub-periosteal part of bone. The visibility of collagenous fibers and absence of bone mineral was observed, hence the use of the term demineralized matrix. A very fine layer (approximately 20 to 30 μm) of white crystals was observed on the outer periosteal border of DM. The second histomorphological zone, the contact zone of lighter gray color and thickness of 50 μm, was observed on the opposite, endosteal, border of the demineralized matrix (Figure 1A, 1B). The CZ was observed as an interface between the demineralized and mineralized matrix, hence the choice of the term. A higher magnification view of the crystals that precipitated in the CZ is shown in Figure 1B. The maximal thickness of the crystals in the current slice of the bone is 50 μm, and they precipitated along the 600 μm of the CZ. The last zone is inner and white mineralized matrix. The mineralized matrix has a thickness of approximately 1500 μm (for this particular bone treated in 2M acid for 4 hours), and standard bone histological structures such as lacunae and Haversian/Volkmann's canals are identifiable in this zone. Figure 1C shows a higher magnification view of a Haversian canal in MM but in proximity to the contact zone and precipitated white crystal within the canal. In the current slice of the bone, the crystal appears to be 300 μm thick and 80 μm long. Moreover, there

is a visible darkening of the MM surrounding the canal in Figure 1C. A higher magnification view of another Haversian canal that is closer to the endosteal border of the cross section and does not contain any crystals is presented in Figure 1D. The edges of the Haversian canal in Figure 1D are sharp, and there is no darkened area surrounding it.

Statistics of total cortical thickness of acid-treated and control samples in relation to concentration and time are presented in Figure 3 and Table 1. The mean of total cortical thickness in controls in the medial and lateral anatomical regions was 2417.9 μm and 2426.9 μm, respectively, approximately twice as thick as in the anterior and posterior anatomical regions, which were 1263.5 μm and 1366.7 μm, respectively. The mean of total cortical thickness decreased by 5%–35% between control and acid-treated bones when each anatomical region was analyzed separately: a 5% decrease was observed for bones from the medial side treated in 0.5 M HCl for 2 h, and a 35% decrease was observed for bones also from the medial side treated in 2 M HCl for 2 h. The largest difference in the mean of total cortical thickness between acid-treated and control samples was in the lateral anatomical region for all acid-treated bones pooled. The mean of total cortical thickness in acid-treated bones decreased significantly in relation to acid concentration ($p = 0.04$) and non-significantly in relation to time of immersion ($p = 0.32$).

Statistics of demineralized matrix thickness relative to acid concentration and time of immersion are shown in Figure 4A and Table 2A. The mean of DM thickness (for pooled anatomical regions) increased 67% between samples treated in 0.5 M acid for 2 h and samples treated in 2 M acid for 4 h. The largest mean increase in the DM thickness was in the anterior anatomical region (70%), whereas the smallest increase was in the lateral anatomical region (63%). The difference between the thickest and thinnest anatomical regions in the demineralized matrix (when pooling all acid treatments) was 45% (anterior and lateral, respectively). The mean

of DM thickness increased significantly with increasing acid concentration ($p < 0.001$) as well as with increasing time of immersion ($p < 0.001$). When the time of acid immersion was doubled and the acid concentration halved from the original, the DM thickness values were similar. The mean difference of DM thickness in samples exposed to 1 M acid for 2 h and samples exposed to 0.5 M acid for 4 h was 5% for pooled anatomical regions. The mean difference in DM thickness in samples exposed to 2 M acid for 2 h and samples exposed to 1 M acid for 4 h was 8% for pooled anatomical regions.

Figure 4B and Table 2B show the statistics of contact zone thickness relative to acid concentration and time of immersion. The mean of CZ thickness increased significantly with increasing acid concentration ($p < 0.01$) and increasing time of immersion ($p < 0.001$). Mean of contact zone thickness increased by 56% in the samples treated in 0.5 M acid for 2 h and samples treated in 2 M acid for 4 h for pooled anatomical regions. The largest mean increase in the CZ thickness was in the anterior anatomical region (55%), whereas the smallest increase was in the medial anatomical region (29%). The difference between the thickest and thinnest anatomical regions in the CZ, when pooling all acid treatments, was 25% (medial and lateral anatomical regions, respectively).

Statistics of mineralized matrix thickness relative to acid concentration and time of immersion are included in Figure 4C and Table 2C. The mean of MM thickness decreased significantly with increasing acid concentration ($p < 0.001$) as well as with increasing time of immersion ($p < 0.001$). When the time of acid immersion was doubled and the acid concentration halved from the original, MM thickness values remained similar to those of demineralized matrix. The mean of mineralized matrix thickness decreased by 32% in samples treated in 0.5 M acid for 2 h and samples treated in 2 M acid for 4 h for pooled anatomical regions. Anatomical

regions were also analyzed separately. The anterior anatomical region had the largest decrease (41%), whereas the lateral anatomical region had the smallest decrease (18%), in mean of MM thickness. We also compared the anterior and lateral anatomical regions by pooling all acid-treated bones within each anatomical region. The difference between the MM thickness of the thickest (lateral) and thinnest (anterior) anatomical regions was 18%.

. Chemical changes

The ratio of calcium to phosphorus (Ca:P) was detected for the contact zone (CZ) and mineralized matrix (MM). In the demineralized matrix (DM), there were no traces of phosphorus and only some traces of calcium detected. Therefore, no Ca:P ratio could be calculated for the DM, which supports our histomorphological observations of color change and collagen fiber exposure in the DM.

Statistics for the Ca:P ratio in mineralized matrix of acid-treated and control samples in relation to acid concentration and time of immersion are shown in Figure 5A and Table 3A. No significant effect of acid concentration ($p = 0.23$) or time of immersion ($p = 0.40$) on the Ca:P ratio in MM was observed. In the MM, the mean difference in the Ca:P ratio between acid-treated bones and controls ranged from 0.03% to 3% depending on anatomical region. The largest difference in mean of Ca:P ratio in MM between the controls and samples treated in 2 M acid for 4 h was in the anterior anatomical region.

Figure 5B and Table 3B show statistics for the Ca:P ratio in the contact zone in relation to acid concentration and time of immersion. The Ca:P ratio of the CZ decreased by 10% compared to the Ca:P ratio of MM in acid-treated samples for pooled anatomical regions. When comparing the differences for each anatomical region separately, the largest decrease between the mean of Ca:P ratio in controls and the CZ was 12% and occurred in the lateral anatomical region. The smallest decrease between the mean of Ca:P ratio in controls and the CZ was 5% and occurred in

the medial anatomical region. The values of the 95% confidence interval for the Ca:P ratio in the CZ of samples immersed in acid for 4 h increased with increasing concentration in all anatomical regions.

We also analyzed the Ca:P ratio for crystals in the CZ, and the results are presented in Table 4. The mean of Ca:P ratio for four random crystals in the CZ was 1.03 (SD = 0.061), which is different from the standard Ca:P ratio of hydroxyapatite (1.67) and very similar to Ca:P values of brushite or monetite (1.00

Number and area of crystals

Statistics for crystal number are presented in Table 5A. Table 5A contains standardized values (mean number of crystals per 1 mm^2 of CZ) due to changing contact zone thickness relative to acid concentration and absolute values (number of bones in which crystals were found). Statistics for crystal area are presented in Table 5B, which also contains standardized values of crystal area per 1 mm^2 of CZ together with the absolute values of the number of bones in which the crystals were found. We observed crystals present in the contact zone and in mineralized matrix within Haversian/Volkmann's canals. The crystals from the contact zone were analyzed further in acid-treated bones. The crystals were present in all acid-treated samples except for the anterior anatomical region in the 0.5 M/2 h acid treatment. Overall, the lowest number of crystals present in the CZ was in subsamples exposed to the 0.5 M concentration.

Statistics for absolute mean values of crystal number in the CZ in relation to acid concentration and time of immersion are shown in Figures 6A and 6B. The crystal number mean is calculated for pooled anatomical regions. Absolute mean values of crystal number increased with concentration and time. The average increase in crystal number was steeper with increasing

concentration than with increasing time. Similarly, statistics for absolute mean values of crystal area in the CZ in relation to acid concentration and time of immersion for pooled anatomical regions are plotted in Figures 6C and 6D. The mean values of crystal area increased with time and concentration; however, the effect of concentration on the increase in crystal area was larger than the effect of time of immersion. The average increase in crystal area between the 1 M and 2 M concentrations was larger than the increase between the 0.5 M and 1 M concentrations.

Table 5A and Figure 7A show statistics for standardized crystal number in the CZ grouped by anatomical location and acid concentration and time of immersion. The mean of crystal number increased significantly in relation to acid concentration ($p < 0.001$). The largest increase in mean of crystal number (93%) was observed in the medial anatomical region between 0.5 M acid and 2 M acid in samples immersed for 2 h. Regardless of acid concentration and time of immersion, the anterior anatomical region of the CZ contained the lowest number of crystals, whereas the medial anatomical region of the CZ contained the largest crystal number (the difference was 61%). The increase in crystal number between anterior and medial anatomical regions was between 47% and 100%. The mean of crystal number actually decreased with increasing time of immersion for the samples treated in 2 M acid. The mean of crystal number did not change significantly in relation to time of immersion ($p = 0.93$) despite the significant increase in the mean of crystal area with time. The decreases in the mean of crystal numbers between the 2 M/2 h samples and 2 M/4 h samples were 1% for the anterior anatomical region, 18% for the lateral anatomical region, and 20% for the posterior and medial anatomical regions.

Statistics of crystal area per 1 mm^2 of contact zone in relation to acid concentration and time of immersion are shown in Table 5B and Figure 7B. The mean of crystal area increased significantly ($p < 0.001$) with increasing acid concentration. The largest increase in mean of

crystal area (98%) was observed between 0.5 M acid and 2 M acid in samples immersed for 2 h in the medial anatomical region. The mean of crystal area increased significantly ($p < 0.001$) also with increasing time of immersion. The largest increase (92%) in the mean of crystal area between samples with the same concentration (2 M) and two immersion times (2 h, 4 h) was in the anterior anatomical region.

Crystals in the contact zone visualized by micro CT are included in Figure 8. Micro CT was employed to gain better spatial visualization of crystals within acid-treated bone. The number of crystals analyzed in the sample was 312. The smallest detected crystals had at least 16 voxels (voxel size 2 μm). The total calculated volume of the crystals was 31.83×10^6 μm^3. All observed crystals were situated in the bone vascular system. Additionally, most of the crystals were situated at the interface between the mineralized matrix and contact zone.

Discussion

Our results demonstrated that the exposure to hydrochloric acid caused morphological and chemical changes in bone on the histological level. Hydrochloric acid exposure caused the formation of three distinct layers in cortical tissue transverse cross section and was also demonstrated by leaching of phosphorus and calcium out of mineralized matrix. In the periosteal part, there was demineralized matrix; in the endosteal part, there remained mineralized matrix; and between the demineralized and mineralized matrix, the contact zone was observed. With increasing acid concentration and time of immersion, the thickness of the demineralized matrix and contact zone increased, whereas the thickness of mineralized matrix decreased. Demineralized matrix contained only traces or no calcium and no phosphorus. In the contact zone, the mean of Ca:P ratio (between 1.40 and 1.50) was lower than the mean of Ca:P ratio in mineralized matrix (between 1.53 and 1.60). Moreover, our results also show precipitation of

crystals on the periosteal surface of demineralized matrix, in the contact zone, and within the Haversian/Volkmann's canals of mineralized matrix. The crystals in the contact zone of acid-treated bones increased in number and size with increasing acid concentration and time of immersion. Furthermore, bone micro-degradation by hydrochloric acid progressed differently among the anterior, posterior, medial, and lateral anatomical regions. For example, the decrease in thickness of mineralized matrix due to acid immersion was 41% in the anterior anatomical region and 18% in the lateral anatomical region.

Two zones, demineralized and mineralized matrix, that we observed in acid-treated bones are in agreement with findings of Lewandrowski et al. (1997) and Horneman et al. (2004) who report both of these in bone cross sections after hydrochloric acid treatment. However, we also observed the presence of a third structure, the contact zone. Lewandrowski et al. (1997) mention an interface at the reaction front between the demineralized and non-demineralized portions of the bone with a thickness of 20 μm; however, they do not report whether it remains stable or changes with acid concentration/time of immersion. Given that we used a more complex project design (three acid concentrations and two immersion durations) and advanced SEM techniques (higher magnification and BSE mode), we identified this interface as a separate zone with some of its properties (Ca:P ratio between 1.4 and 1.5, thickness between 16 and 43 μm) dependent on acid concentration, time of acid immersion, and anatomical regions.

We observed Ca:P ratio values in mineralized matrix with a mean range between 1.53 and 1.60. This indicates the presence of intact hydroxyapatite in our mineralized matrix despite our values for Ca:P ratio being at the lower end observed for hydroxyapatite by Hancox (1972) (between 1.5 and 1.67). The slightly lower Ca:P ratios observed in our mineralized matrix may

be a product of natural variation due to variable hydroxyapatite crystal sizes or hormonal influence (Hancox, 1972).

We observed that in the contact zone, the hydroxyapatite Ca:P ratio decreased significantly compared to the Ca:P ratio of mineralized matrix, to mean values between 1.41 and 1.45 (pooled anatomical regions). Similarly, El-Bassyouni et al. (2013) report reduced amounts of calcium and phosphorus, to one-third and one-tenth of the control measurements, in canine bones demineralized in hydrochloric acid. It is suggested that demineralization by hydrochloric acid could cause distortions of hydroxyapatite crystal size, which is reported in Danilchenko et al. (2003) in experiments with bovine bones. As mentioned by Hancox (1972), the Ca:P ratio is influenced by hydroxyapatite crystal size. Therefore, a decrease in the hydroxyapatite Ca:P ratio in the contact zone might possibly be caused by reported hydroxyapatite crystal size changes during demineralization by hydrochloric acid.

Hydroxyapatite in acid-treated bones has a potential to recrystallize to brushite crystals (Oliveira et al., 2007). Hydroxyapatite exposed to acidic treatment can also recrystallize to monetite, which is a monocyclic form of brushite (Tamimi et al., 2012). In our study, recrystallization of bone hydroxyapatite to brushite is documented by decreased Ca:P ratio values. The mean Ca:P ratio value of crystals observed in the contact zone (1.03) in our study appears to be in agreement with values of 1.00 for brushite and monetite reported by Poštić (2014). However, X-ray diffraction would be necessary to confirm the exact identification of the crystals present as either brushite or monetite. Similar observations of bone hydroxyapatite recrystallization into brushite were provided by other researchers; for example, the presence of brushite was described on bones exposed to acidic environments in forensic cases (Thurzo, 1993). Also, Schotsmans et al. (2017) report brushite and monetite identification in

archaeological bone samples. Recrystallization of hydroxyapatite into brushite is in accordance with Oliveira et al. (2007) who observed hydroxyapatite exposed to acidic conditions and its transformation into brushite *in vitro* via X-ray diffraction. Lee-Thorp and van der Merwe (1991) report formation of brushite in bone experimentally immersed in acetic acid. Moreover, Piepenbrink (1989) explains the formation of brushite during bone fossilization as a result of hydroxyapatite recrystallization after it was dissolved in acidic soils.

Hydrochloric acid has a potential to advance through bone tissue as a front in the form of the contact zone. Front-like advancement of hydrochloric acid was confirmed by Lewandrowski et al. (1997), who mention a uniformly advancing interface between demineralized and non-demineralized parts of bone. However, besides an advancing front of the contact zone, we also observed crystals within the Haversian/Volkmann's canals in the mineralized matrix. Moreover, 3D visualization of the contact zone shows close association of brushite present there with remnants of vascular canals in this zone (Figure 7). Therefore, it appears that acid advances through bone tissue as a front, but to some extent, it also traverses through the tissue respecting its vascular histomorphology prior to the front line.

We observed that increasing hydrochloric acid concentration and time of immersion caused increased cortical bone demineralization. We demonstrated the effects of concentration and time as an increase of 67% in the thickness of demineralized matrix and an increase of 56% in the thickness of the contact zone between samples treated in 0.5 M acid for 2 h and in 2 M acid for 4 h. Consequently, the thickness of mineralized matrix decreased by 27% with increasing acid concentration and time. The effect of hydrochloric acid concentration on bone demineralization was also observed by calculation of linear kinetic profiles of demineralized samples in Figueiredo et al. (2011). Figueiredo et al. (2011) confirmed the trend of increasing

rate of bone demineralization with increasing concentration of hydrochloric acid in human bone samples, but the demineralization rate observed in their study was more pronounced when the concentration increased from 0.6 M to 1.2 M than when the concentration increased from 1.2 M to 2.4 M. The effect of time of immersion in hydrochloric acid on bone demineralization was observed by Hartnett et al. (2011), who measured the rate of demineralization by bone weight loss. They confirmed the longer the bone was exposed to the acid, the larger the tissue weight loss was, which is consistent with the increasing loss of mineralized matrix with longer acid immersion in our study.

We observed that anatomical regions were a critical factor in the demineralization of cortical bone by hydrochloric acid. The impact of acid among anatomical regions differed in demineralized/mineralized matrix and contact zone thicknesses and in number/size of crystals within the contact zone. For example, the thickness of mineralized matrix and contact zone in the anterior anatomical region changed by 41% and 51%, respectively, when comparing the 0.5 M/2 h and 2 M/4 h acid treatments. On the other hand, the thickness of the mineralized matrix and contact zone in the medial anatomical region changed by 19% and 29%, respectively, when comparing the 0.5 M/2 h and 2 M/4 h acid treatments. Moreover, crystal numbers in the contact zone of the medial anatomical region were approximately two to five times higher than those of the anterior anatomical region (Table 5). One of the explanations for the differences in demineralization between the anatomical regions could be differences in histomorphology of porcine bone. Martiniaková et al. (2006) and Morris (2007) report the presence of histomorphological differences (osteon number and size, presence/absence of plexiform bone) within the tissue of porcine and bovine bone cross sections. Moreover, variable bone histomorphology in cross section was reported in other species, such as turkey (Skedros et al.,

2003), mouse (Jindrová et al., 2016) and human (Pfeiffer, 1998; Goldman et al., 2009). Therefore, histomorphological differences within bone cross sections should be considered when analyzing the impact of demineralization by hydrochloric acid in potential forensic experiments and cases.

The taphonomic pathways and impact of acidic bone decomposition can differ when the impact is observed on de-fleshed or on fleshes bone surrounded by soft tissues (e.g. Janjua and Rogers (2008). Direct impact of acid on de-fleshes bone can be associated with specific forensic cases and environment. For example, Bell et al. (1996) report localized post-mortem demineralization of skeletal remains caused by decomposing gut which naturally contains hydrochloric acid. Further, passing of fleshed and partially de-fleshed bones through digestive tract of other animals is another example of taphonomic pathway which results into bone macro and microdegradation via hydrochloric acid (Fernández-Jalvo et al., 2011; Fernández-Jalvo and Andrews, 2016). On the other hand, decomposition of bone included in soft body tissues may differ from our observed pattern and may be degraded also by agents different to acid. For example, Rodriguez III and Bass (1985) report decreasing acidity (increase in pH) of soil where soft tissue is decomposing. Thus, fleshed bone may undergo changes by following different taphonomic pathways mainly based on the impact of alkaline solution. However, this difference has to be elucidated in future research to help identify histomorphological differences between acid and alkaline bone decomposition.

The results of this study can be utilized in forensic practice despite the different histomorphology of porcine and human bone. Mammalian models are commonly used in taphonomic experiments as a replacement for human material due to ethical and practical considerations (Carter et al., 2010; Schotsmans et al., 2012; Boaks et al., 2014; White and Booth,

2014). The histological morphology of the porcine bones differs from that of human bones in the presence of plexiform bones, smaller number of osteons and larger Haversian/Volkmann's canals (Martiniaková et al., 2006; Morris, 2007). Different bone histomorphology in porcine bones could influence the mode and speed of acid advancement through the tissue. Despite the differences between human and porcine bone tissue, according to the research of Karr and Outram (2015) and Kontopoulos et al. (2016), pig bones are still considered to degrade in a way similar to that of human bones and are utilized in bone degradation research as suitable models. Moreover, Figueiredo et al. (2011) studied the influence of hydrochloric acid concentration using human bone samples. Although their samples differ histomorphologically from those in the current study, the trend of increased demineralization with increasing acid concentration together with chemical changes of mineralized tissue remain similar to the current results and suggest a similar mechanism of degradation by hydrochloric acid in human bones.

Conclusion

After the immersion in hydrochloric acid, we observed changes in bone cross section appearance: a dark gray demineralized matrix was observed in the periosteal part, followed by a thinner light gray contact zone, and a white mineralized matrix in the endosteal part. With increasing acid concentration and time of immersion (comparing 0.5 M/2 h acid with 2 M/4 h acid and pooling all anatomical regions), the thickness of demineralized matrix and contact zone increased (from 127 μm to 384 μm and from 17 μm to 39 μm, respectively), whereas the thickness of mineralized matrix decreased (from 799 μm to 583 μm). The three zones also differed in the hydroxyapatite Ca:P ratio. The Ca:P ratio of demineralized matrix could not be expressed, as almost no phosphorus and only traces of calcium were present in this zone. The Ca:P ratio of the contact zone decreased (from 1.6 to 1.4) in comparison to the Ca:P ratio of

mineralized matrix when among the samples treated in the 2 M/4 h acid and pooled for all anatomical regions. The Ca:P ratio of endosteal mineralized matrix in acid-treated bones was not significantly different from the Ca:P ratio of mineralized matrix in control samples.

Crystals were observed in acid-treated samples on the periosteal surface of the demineralized matrix, within the contact zone, and within the Haversian/Volkmann's canals of mineralized matrix. The Ca:P ratio of crystals in the contact zone categorizes them as either brushite or monetite. Crystals in the contact zone increased in number (8 to 122 crystals per 1 mm^2 of contact zone) and area (700 to 58,000 μm^3 per 1 mm^2 of contact zone) with increasing acid concentration and time of immersion (comparing 0.5 M/2 h acid with 2 M/4 h acid and pooling all anatomical regions).

The anatomical regions differed in the thicknesses of the three zones. The difference between the thickest and thinnest anatomical regions (when pooling all acid treatments) was 45% in demineralized matrix (anterior and lateral, respectively), 25% in the contact zone (medial and lateral, respectively), and 18% in mineralized matrix (lateral and anterior, respectively). The difference between anatomical regions in acid-treated samples was also evident for the number and area of crystals in the contact zone. The anterior anatomical region contained the lowest number of crystals in the contact zone, whereas the medial anatomical region contained the largest number of crystals in the contact zone. The difference in crystal number between the anterior and medial anatomical regions (when pooling all acid treatments) was 61%. Based on our results, the inclusion of separate analyses for each anatomical region might be helpful in potential taphonomic and forensic investigations into hydrochloric acid exposure.

Declarations of interest: none

Acknowledgements

The authors are thankful to Jiří Sluka for the access to the material, to Simona Čerevková and Michal Struška for practical help with sample preparation and data collection, and to Martin Racek and Radim Jedlička from the Institute of Petrology and Structural Geology (Charles University) for their assistance with sample scanning. The authors would like to thank Tomáš Zikmund for his assistance with the application of micro CT in this project. Furthermore, the authors are grateful to Martin Hora and Eline Schotsmans for their helpful comments and advice regarding the project design. This research was supported by The Czech Science Foundation under the project GAČR 18-15480S Death, burials, and skeletons: funeral archaeology and human taphonomy of the new 2nd church cemetery at Pohansko (Břeclav). This research was carried out under the project CEITEC 2020 (LQ1601) with financial support from the Ministry of Education, Youth and Sports of the Czech Republic under the National Sustainability Programme II and support of CEITEC Nano Research Infrastructure (MEYS CR, 2016–2019).

Veronika Sabolová: Conceptualization, Formal analysis, Investigation, Writing – Original draft. **Adam Brinek**: Investigation, Writing – Original draft, Visualisation. **Vladimír Sládek**: Conceptualization, Writing – Review and Editing, Supervision, Funding acquisition.

References

Bell LS, Skinner MF, Jones SJ. 1996. The speed of post mortem change to the human skeleton and its taphonomic significance. Forensic Sci Int 82:129–140.

Boaks A, Siwek D, Mortazavi F. 2014. The temporal degradation of bone collagen: A histochemical approach. Forensic Sci Int 240:104–110.

Carter DO, Yellowlees D, Tibbett M. 2010. Moisture can be the dominant environmental parameter governing cadaver decomposition in soil. Forensic Sci Int 200:60–66.

Castro-Ceseña AB, Novitskaya EE, Chen P, Hirata GA, Mckittrick J. 2011. Kinetic studies of bone demineralization at different HCl concentrations and temperatures. Mater Sci Eng C 31:523–530.

Child AM, Gillard RD, Pollard AM. 1993. Microbially-induced promotion of amino acid racemization in bone: isolation of the microorganisms and the detection of their enzymes. J Archaeol Sci 20:159–168.

Christensen AM, Myers SW. 2011. Macroscopic observations of the effects of varying fresh water pH on bone. J Forensic Sci 56:475–479.

Collins MJ, Nielsen-Marsh CM, Hiller J, Smith CI, Roberts JP, Prigodich R V, Wess TJ, Csapo J, Millard AR, Turner-Walker G. 2002. The survival of organic matter in bone: a review. Archaeometry 44:383–394.

Cope DJ, Dupras TL. 2009. The effects of household corrosive chemicals on human dentition. J Forensic Sci 54:1238–1246.

Danilchenko SN, Moseke C, Boelling O, Pavlenko PA, Stachura Z, Sukhodub LF, Sulkio-Cleff

B. 2003. X-ray analysis of lattice microdistortions and crystallite size in bone mineral under model demineralization. Mineral J 25:65–71.

Denys C. 2002. Taphonomy and experimentation. Archaeometry 44:469–484.

Donaldson AE, Lamont IL. 2013. Biochemistry changes that occur after death: potential markers for determining post-mortem interval. PLoS One 8:e82011.

El-Bassyouni GT, Guirguis OW, Abdel-Fattah WI. 2013. Morphological and macrostructural studies of dog cranial bone demineralized with different acids. Curr Appl Phys 13:864–874.

Fernández-Jalvo Y, Andrews P, Pesquero D, Smith C, Marín-Monfort D, Sánchez B, Geigl EM, Alonso A. 2010. Early bone diagenesis in temperate environments. Part I: Surface features and histology. Palaeogeogr Palaeoclimatol Palaeoecol 288:62–81.

Fernández-Jalvo Y, Andrews P. 2016. Atlas of Taphonomic Identifications. Dordrecht: Springer Netherlands.

Fernández-Jalvo Y, Scott L, Andrews P. 2011. Taphonomy in palaeoecological interpretations. Quat Sci Rev 30:1296–1302.

Figueiredo M, Cunha S, Martins G, Freitas J, Judas F, Figueiredo H. 2011. Influence of hydrochloric acid concentration on the demineralization of cortical bone. Chem Eng Res Des 89:116–124.

Goldman HM, Mcfarlin SC, Cooper DML, Thomas CDL, Clement JG. 2009. Ontogenetic patterning of cortical bone microstructure and geometry at the human mid-shaft femur. Anat Rec Adv Integr Anat Evol Biol 292:48–64.

Goldschlager T, Abdelkader A, Kerr J, Boundy I, Jenkin G. 2010. Undecalcified bone preparation for histology, histomorphometry and fluorochrome analysis. J Vis Exp:1707.

Hancox NM. 1972. Biology of Bone. Cambridge: Cambridge University Press.

Hartnett KM, Fulginiti LC, Di Modica F. 2011. The effects of corrosive substances on human bone, teeth, hair, nails, and soft tissue. J Forensic Sci 56:954–959.

Hedges REM, Millard AR. 1995. Bones and groundwater: towards the modelling of diagenetic processes. J Archaeol Sci 22:155–164.

Hedges REM. 2002. Bone diagenesis: an overview of processes. Archaeometry 44:319–328.

Higgs ND, Glover AG, Dahlgren TG, Little CT. 2011. Bone-boring worms: characterizing the morphology, rate, and method of bioerosion by Osedax mucofloris (Annelida, Siboglinidae). Biol Bull 221:307–316.

Hollund HI, Ariese F, Fernandes R, Jans MME, Kars H. 2012. Testing an alternative high-throughput tool for investigating bone diagenesis: FTIR in attenuated total reflection (ATR) mode. Archaeometry 55:507–532.

Hopkins DW, Wiltshire PEJ, Turner BD. 2000. Microbial characteristics of soils from graves: an investigation at the interface of soil microbiology and forensic science. Appl Soil Ecol 14:283–288.

Horneman DA, Ottens M, Hoorneman M, van der Wielen LAM, Tesson M. 2004. Reaction and diffusion during demineralization of animal bone. AIChE J 50:2682–2690.

Janjua MA, Rogers TL. 2008. Bone weathering patterns of metatarsal v. femur and the

postmortem interval in Southern Ontario. Forensic Sci Int 178:16–23.

Jans MME, Nielsen-Marsh CM, Smith CI, Collins MJ, Kars H. 2004. Characterisation of microbial attack on archaeological bone. J Archaeol Sci 31:87–95.

Jindrová A, Tuma J, Sládek V. 2016. Impact of non-invasively induced motor deficits on tibial cortical properties in mutant lurcher mice. PLoS One 11:e0158877.

Karnovsky MJ. 1965. A formaldehyde-glutaraldehyde fixative of high osmolarity for use in electron microscopy. J Cell Biol 27:1A–149A.

Karr LP, Outram AK. 2015. Bone degradation and environment: understanding, assessing and conducting archaeological experiments using modern animal bones. Int J Osteoarchaeol 25:201–212.

King CL, Tayles N, Gordon KC. 2011. Re-examining the chemical evaluation of diagenesis in human bone apatite. J Archaeol Sci 38:2222–2230.

Kontopoulos I, Nystrom P, White L. 2016. Experimental taphonomy: post-mortem microstructural modifications in Sus scrofa domesticus bone. Forensic Sci Int 266:320–328.

Lee-Thorp JA, van der Merwe NJ. 1991. Aspects of the chemistry of modern and fossil biological apatites. J Archaeol Sci 18:343–354.

Lewandrowski K, Tomford WW, Michaud NA, Schomacker KT, Deutsch TF. 1997. An electron microscopic study on the process of acid demineralization of cortical bone. Calcif Tissue Int 61:294–297.

López-Costas O, Lantes-Suárez Ó, Martínez Cortizas A. 2016. Chemical compositional changes

in archaeological human bones due to diagenesis: type of bone vs soil environment. J Archaeol Sci 67:43–51.

Martiniaková M, Grosskopf B, Vondráková M, Omelka R, Fabiš M. 2006. Differences in femoral compact bone tissue microscopic structure between adult cows (Bos taurus) and pigs (Sus scrofa domestica). J Vet Med Ser C Anat Histol Embryol 35:167–170.

Mazza A, Merlati G, Savio C, Fassina G, Menghini P, Danesino P. 2005. Observations on dental structures when placed in contact with acids: experimental studies to aid identification processes. J Forensic Sci 50:406–410.

Morris ZH. 2007. Quantitative and spatial analysis of the microscopic bone structures of deer (Odocoileus virginianus), dog (Canis familiaris) and pig (Sus scrofa domesticus). Master Arts Thesis, Louisiana State Univ.

Nicholson RA. 1996. Bone degradation, burial medium and species representation: debunking the myths, an experiment-based approach. J Archaeol Sci 23:513–533.

Nielsen-Marsh CM, Hedges REM. 2000. Patterns of diagenesis in bone I: the effects of site environments. J Archaeol Sci 27:1139–1150.

Oliveira C, Georgieva P, Rocha F, Ferreira A, Feyo De Azevedo S. 2007. Dynamical model of brushite precipitation. J Cryst Growth 305:201–210.

Pfeiffer S. 1998. Variability in osteon size in recent human populations. Am J Phys Anthropol 106:219–227.

Piepenbrink H. 1989. Examples of chemical changes during fossilization. Appl Geochemistry 4:273–280.

Poštić SD. 2014. X-ray diffraction technique in the analysis of phases of hydroxylapatite and calcium phosphate in a human jaw. Int J Biomed 4:109–113.

Rodriguez III WC, Bass WM. 1985. Decomposition of buried bodies and methods that may aid in their location. J Forensic Sci 30:836–852.

Ruff CB. 2008. Biomechanical analyses of archaeological human skeletons. In: Katzenberg MA, Saunders SR, editors. Biological Anthropology of the Human Skeleton. Hoboken, NJ, USA: John Wiley & Sons, Inc. p 183–206.

Schindelin J, Arganda-Carreras I, Frise E, Kaynig V, Longair M, Pietzsch T, Preibisch S, Rueden C, Saalfeld S, Schmid B, Tinevez J-Y, White DJ, Hartenstein V, Eliceiri K, Tomancak P, Cardona A. 2012. Fiji: an open-source platform for biological-image analysis. Nat Methods 9:676–682.

Schotsmans EMJ, Denton J, Dekeirsschieter J, Ivaneanu T, Leentjes S, Janaway RC, Wilson AS. 2012. Effects of hydrated lime and quicklime on the decay of buried human remains using pig cadavers as human body analogues. Forensic Sci Int 217:50–59.

Schotsmans EMJ, de Voorde W Van. 2017. Concealing the Crime : the Effects of Chemicals on Human Tissues. In: Schotsmans EMJ, Márquez-Grant N, Forbes SL, editors. Taphonomy of Human Remains: Forensic Analysis of the Dead and the Depositional Environment. 1st ed. Chichester: John Wiley & Sons Ltd. p 335–351.

Skedros JG, Hunt KJ, Hughes PE, Winet H. 2003. Ontogenetic and regional morphologic variations in the turkey ulna diaphysis: Implications for functional adaptation of cortical bone. Anat Rec A Discov Mol Cell Evol Biol 273A:609–629.

Sládek V, Sabolová V, Šebesta O, Zikmund T, Kaiser J, Čerevková S. 2018. Effect of deriving periosteal and endosteal contours from microCT scans on computation of cross-sectional properties in non-adults: the femur. J Anat 233:381–393.

StatSoft Inc. 2015. http://www.statsoft.com.

Tamimi F, Sheikh Z, Barralet J. 2012. Dicalcium phosphate cements: Brushite and monetite. Acta Biomater 8:474–487.

Thurzo M. 1993. Decomposition of skeletal remains caused by dry rot as one of the taphonomic factors. In: Pavúk J, editor. Actes de XIIe Congres International des Sciences Préhistoriques et Protohistoriques Bratislava 1-7 Septembre 1991. Tome 1. Bratislava: Institut archéologique de l'Académie Slovaque des Sciences. p 189–192.

Turner-Walker G. 2007. The Chemical and Microbial Degradation of Bone and Teeth. In: Pinhasi R, Mays S, editors. Advances in Human Palaeopathology. Chichester, UK: John Wiley & Sons Ltd.

Walsh WR, Christiansen DL. 1995. Demineralized bone matrix as a template for mineral-organic composites. Biomaterials 16:1363–1371.

White L, Booth TJ. 2014. The origin of bacteria responsible for bioerosion to the internal bone microstructure: results from experimentally-deposited pig carcasses. Forensic Sci Int 239:92–102.

Zhang M, Powers RM, Wolfinbarger L. 1997. Effect(s) of the demineralization process on the osteoinductivity of demineralized bone matrix. J Periodontol 68:1085–1092.

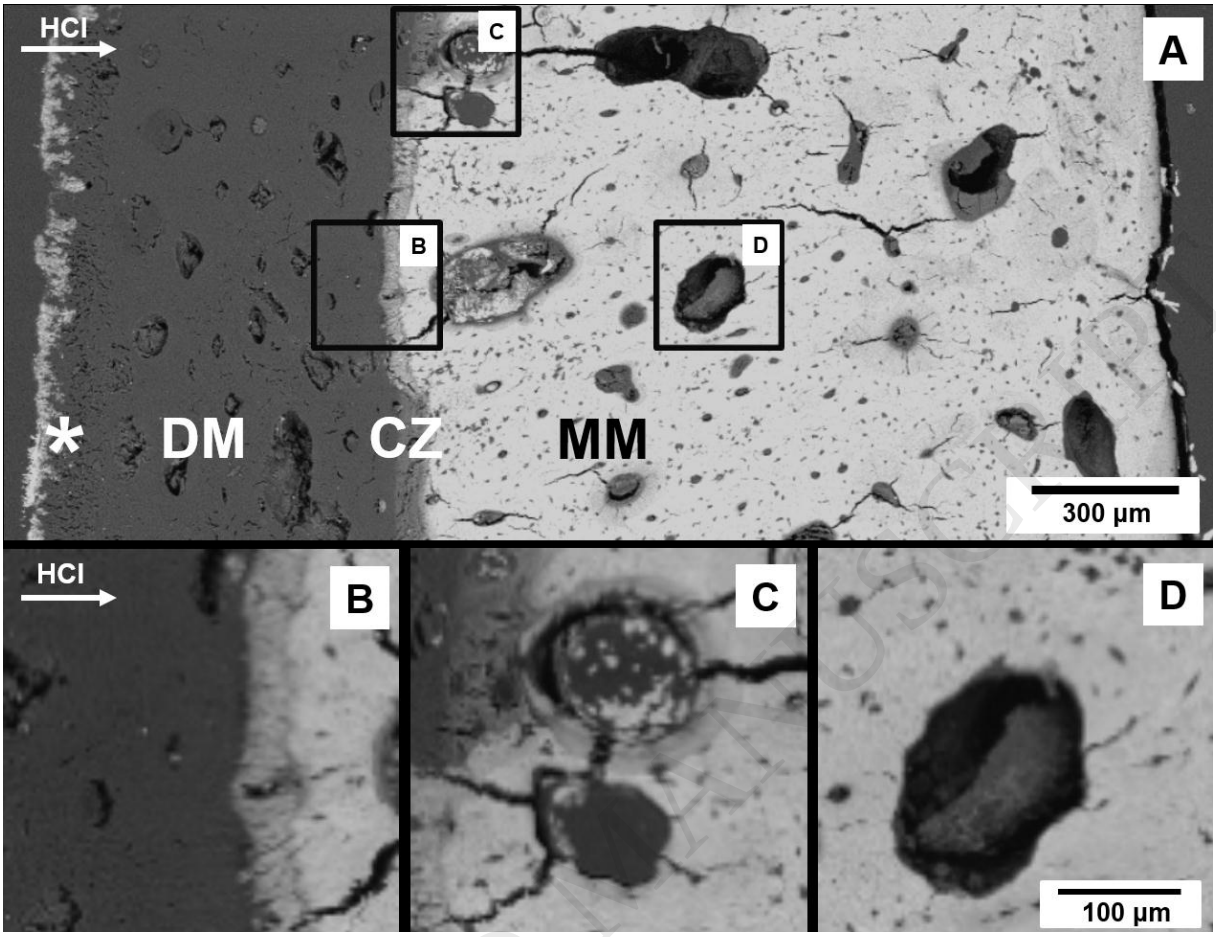

Figure 1. Transverse section of acid-treated bone (2 M/4 h); arrow shows the direction of HCl advance. (A) Higher magnification of the medial anatomical region, 1 = demineralized matrix, 2 = contact zone, 3 = mineralized matrix, * = crystals on periosteal surface. (B) Detail of contact zone. (C) Haversian canal close to the contact zone containing crystals. (D) Haversian canal within mineralized matrix without crystals.

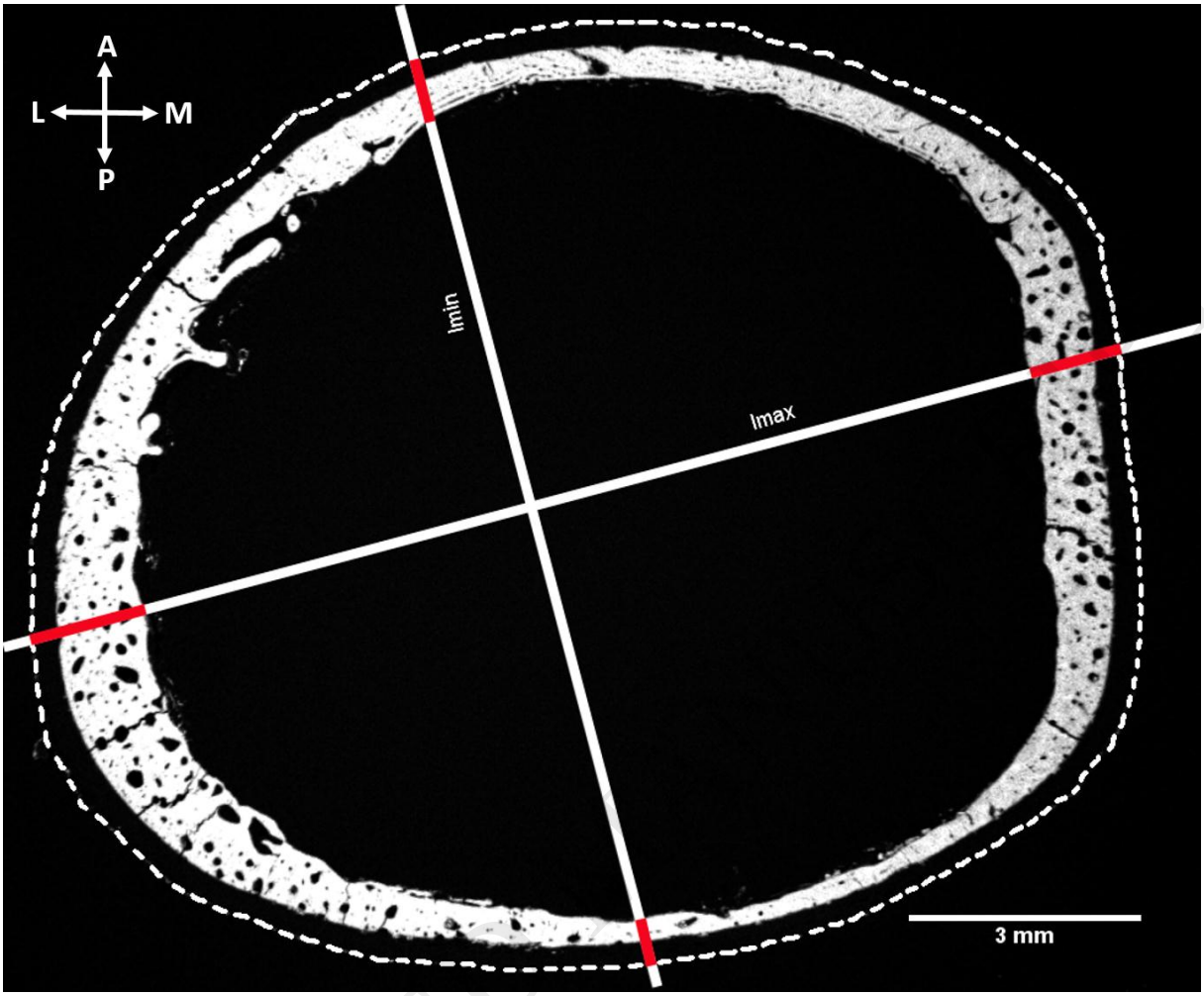

Figure 2: Transverse section of acid-treated bone (2M/2h); I_{max} = axis in maximum second moment of area, I_{min} = axis in minimum second moment of area; red-highlighted sections are locations where total cortical thickness and thicknesses of the histomorphologically distinct zones was measured in relation to anatomical regions (Ant, Post, Med, Lat); dashed line denotes outer border of demineralized matrix.

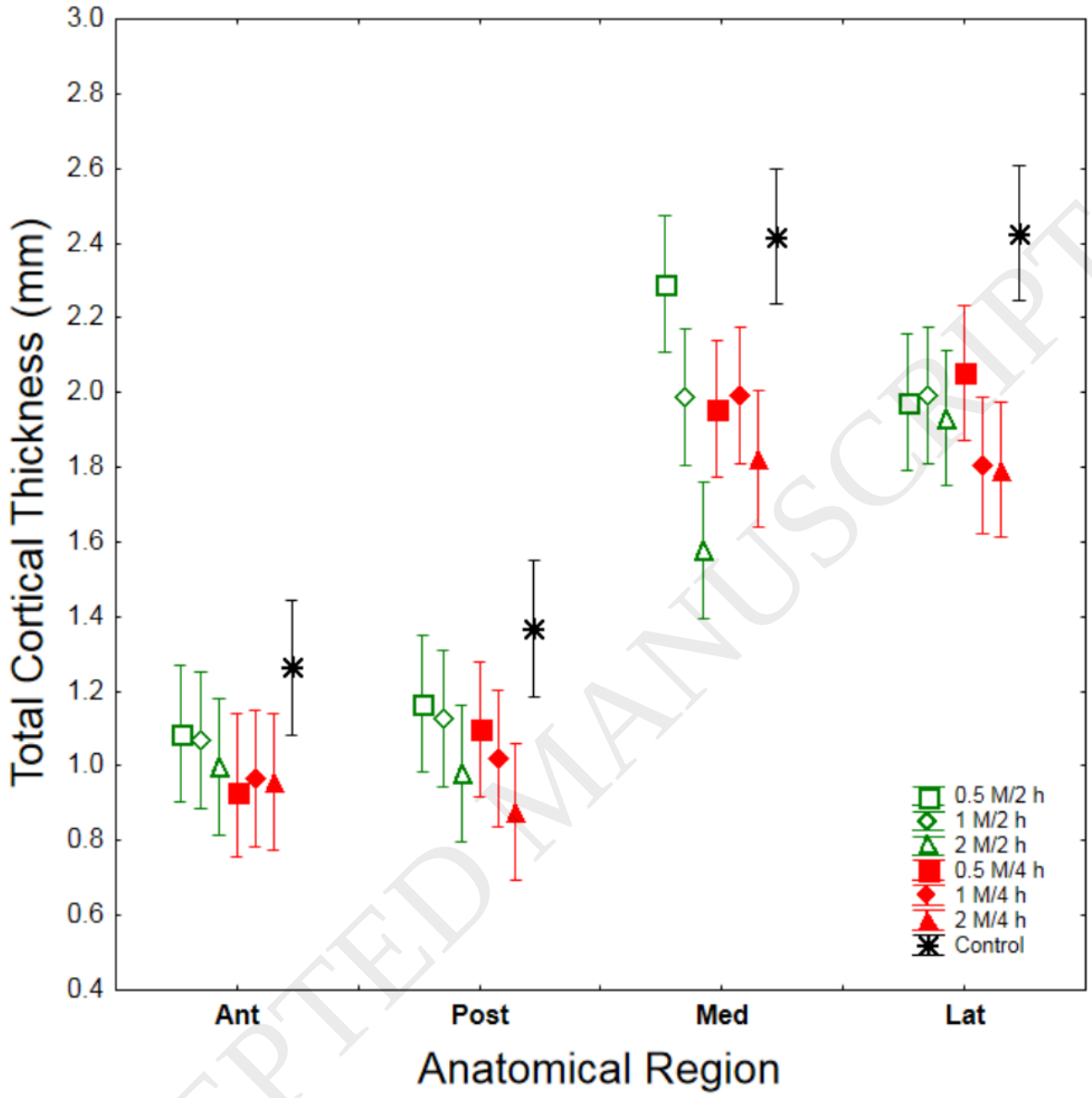

Figure 3. Mean thickness of cortical bone in transverse cross-sections, Ant = anterior, Post = posterior, Med = medial, Lat = lateral. Vertical bars denote ±95% confidence intervals.

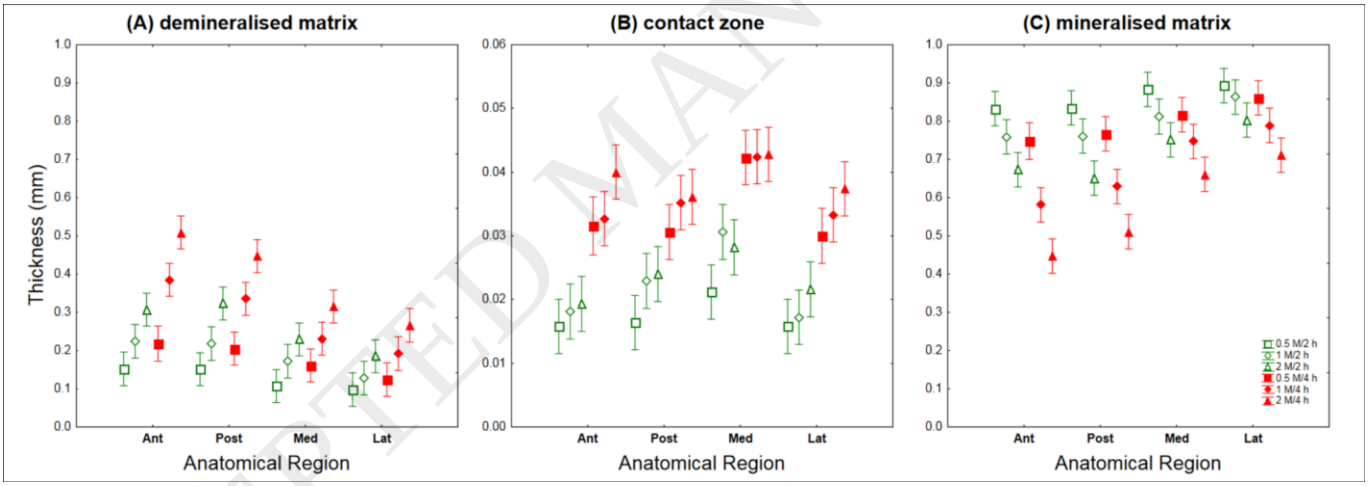

Figure 4. Mean thickness values of cortical bone zones in acid-treated bones. Vertical bars denote ±95% confidence interval. Values of demineralized/mineralized matrix are adjusted by corresponding values of total cortical thickness

).

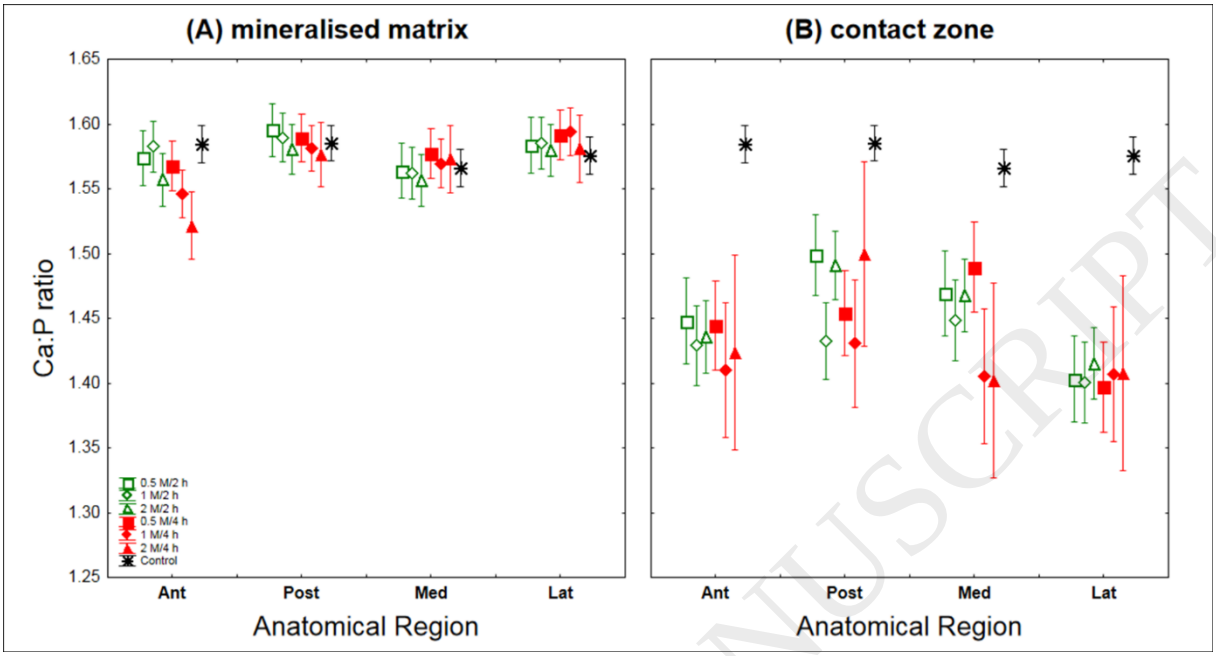

Figure 5. Mean Ca:P values, vertical bars denote ±95% confidence interval. (A) Differences between the mineralized matrix of controls and acid-treated bones. (B) Differences between the mineralized matrix and contact zone of acid-treated bones. (Note: the Ca:P values of collagen in acid-treated bones could not be calculated, as phosphorus was not detected in collagen.)

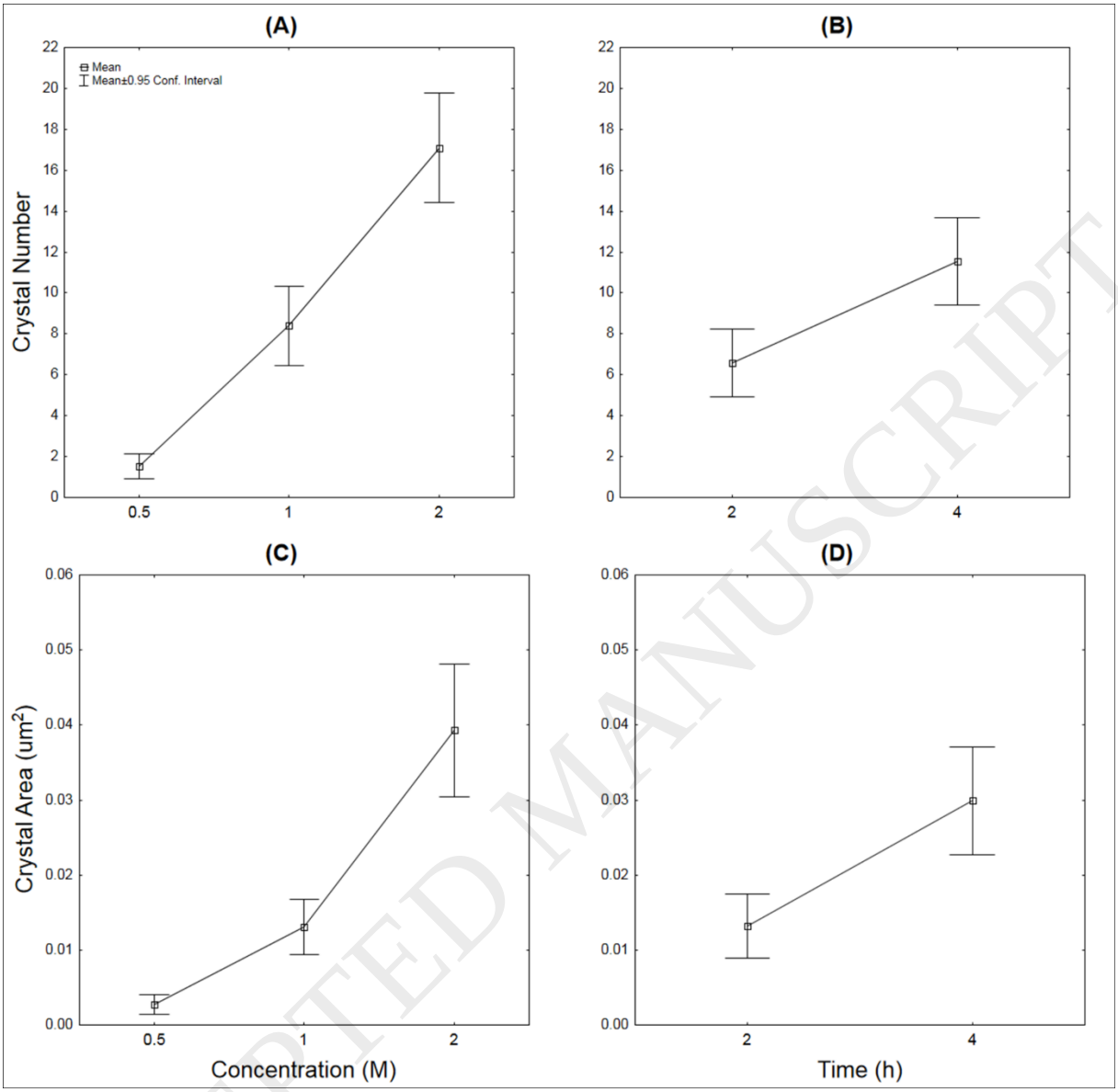

Figure 6. (A) Absolute mean values of crystal number in the contact zone in relation to acid concentration. (B) Absolute mean values of crystal number in the contact zone in relation to time of immersion in acid. (C) Absolute mean values of crystal area in the contact zone in relation to acid concentration. (D) Absolute mean values of crystal number in the contact zone in relation to time of immersion in acid. Vertical bars denote ±95% confidence interval.

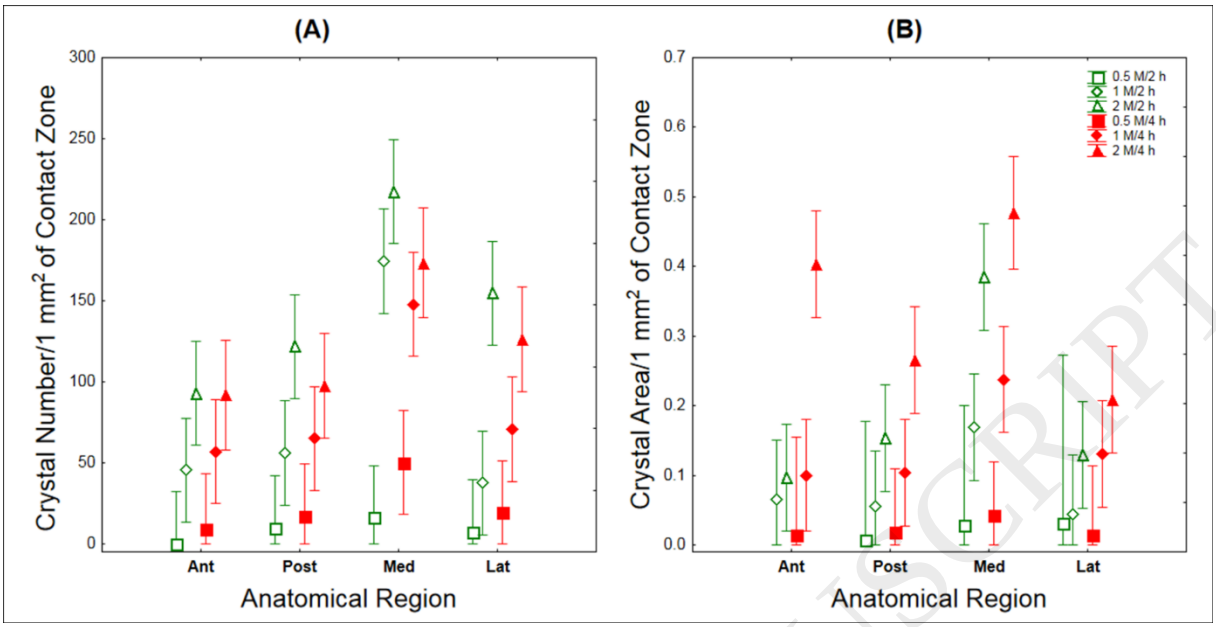

Figure 7. (A) Mean number of crystals per 1 mm^2 of contact zone; $p_{time} = 0.925$, $p_{conc} < 0.001$. (B) Mean area of crystals per 1 mm^2 of contact zone; $p_{time} < 0.001$, $p_{conc} < 0.001$. Vertical bars denote ±95% confidence interval.

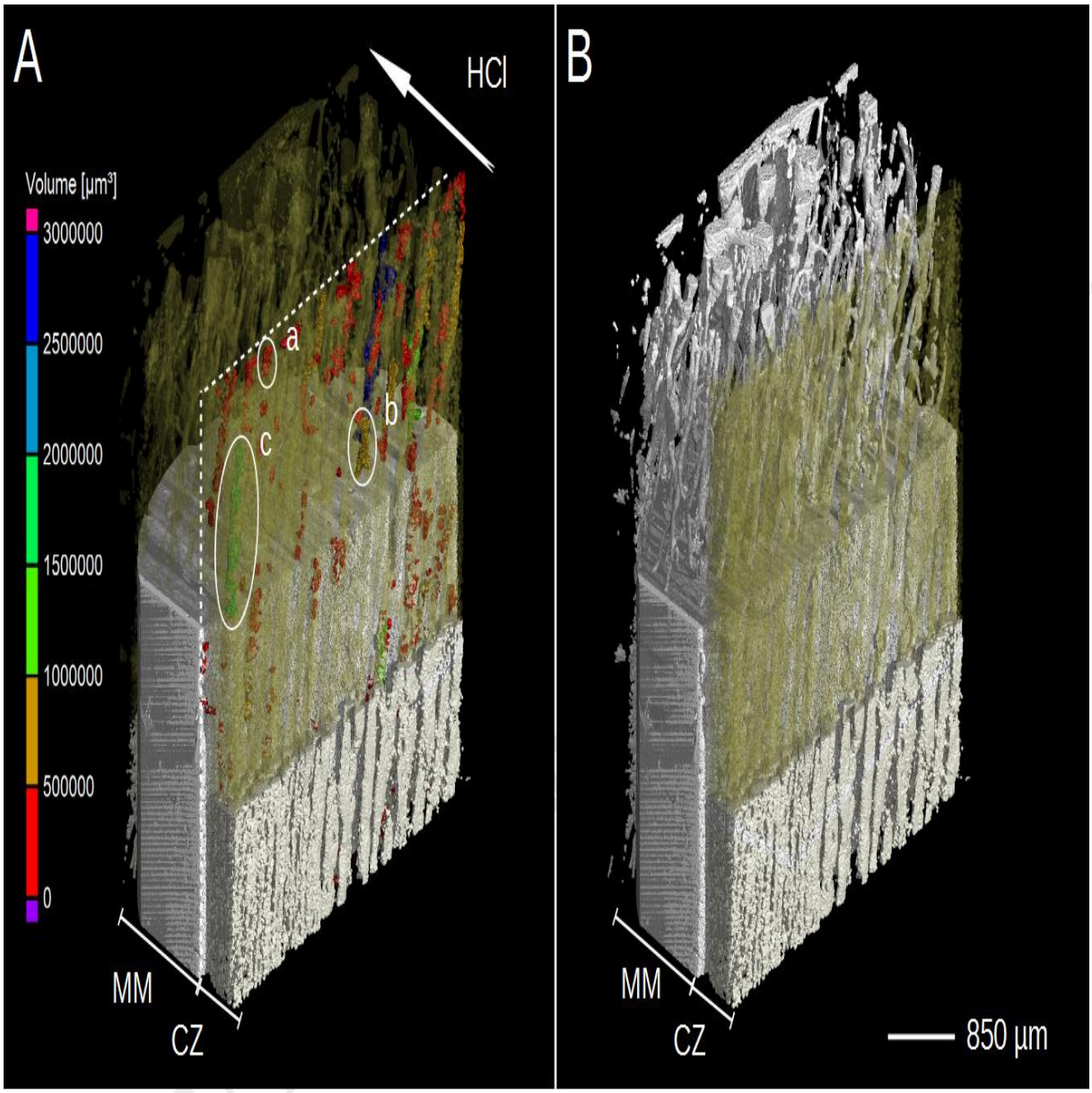

Figure 8. Figure 8. Subsection of medial anatomical region (bone treated in 1 M/2 h HCl) visualized by micro CT. (A) MM = mineralized matrix with its upper one third made 'see-through' to reveal yellow ghost-like inner vascular structures of bone; CZ = contact zone also made 'see-through' in upper two thirds to reveal crystals (a, b, c) which are color-coded according to their volume, white dashed line denotes border between CZ and MM. White arrow shows direction of acid flow through the bone. (B) Cast of vascular structures observed in mineralized matrix (MM).

	2 hours						4 hours							
	0.5 M HCl		1 M HCl		2 M HCl		0.5 M HCl		1 M HCl		2 M HCl		Control	
Region	**Mean**	**±SD**	**Mean**	**±SD**	**Mean**	**±SD**	**Mean**	**±SD**	**Mean**	**±SD**	**Mean**	**±SD**	**Mean**	**±SD**
Anterior	1086.4	187.77	1068.0	256.64	996.9	214.34	946.8	129.08	967.6	169.96	957.5	203.61	1263.5	179.38
Posterior	1167.8	148.66	1127.1	258.08	980.2	254.94	1098.1	156.21	1020.5	137.23	878.8*	139.24	1366.7	201.28
Medial	2289.9	167.67	1987.8	147.45	1576.4*	265.65	1956.9	358.30	1990.9	223.55	1821.6*	248.16	2417.9	285.66
Lateral	1973.2	260.97	1993.5	346.67	1931.5*	500.77	2052.5	404.83	1803.9*	314.24	1793.6*	542.70	2426.9	652.55

Table 1 Statistics of total cortical thickness (μm) in acid-treated and control bone samples. The sample size equals 10 bones per group, except for anterior 0.5 M HCl containing 9 bones. *Acid-treated subsamples significantly different from control within corresponding anatomical region.

		2 hours						4 hours					
		0.5 M HCl		1 M HCl		2 M HCl		0.5 M HCl		1 M HCl		2 M HCl	
Region		**Mean**	**±SD**	**Mean**	**±SD**	**Mean**	**±SD**	**Mean**	**±SD**	**Mean**	**±SD**	**Mean**	**±SD**
Anterior	A	151.84	24.57	223.88	54.58	306.83	65.25	217.84	52.20	384.46	64.29	508.73	212.06
	B	15.80	5.22	18.10	4.82	19.30	3.13	31.60	7.42	32.70	7.09	40.00	6.83
	C	832.98	28.42	758.43	57.97	673.10	68.30	748.37	58.29	581.44	65.08	447.35	216.96

Posterior	A	151.19	31.56	218.16	43.41	323.73	87.00	204.93	21.36	335.22	59.29	447.34	142.34
	B	16.40	4.65	22.90	3.98	24.00	5.50	30.60	7.31	35.20	6.32	36.10	4.41
	C	834.61	33.24	760.75	47.77	650.33	93.76	766.49	25.36	629.56	66.48	510.99	142.80
Medial	A	107.35	22.29	172.23	35.12	229.70	40.39	161.05	24.33	230.74	53.58	315.69	52.79
	B	21.20	9.14	30.60	11.65	28.20	7.25	42.30	8.73	42.4	12.17	42.80	8.47
	C	883.38	25.60	812.11	40.81	751.82	44.98	816.64	27.29	748.00	57.28	660.74	52.66
Lateral	A	98.34	14.44	127.77	27.57	185.32	38.00	124.18	31.65	192.14	66.84	265.83	62.11
	B	15.80	6.70	17.20	3.94	21.60	2.76	30.00	5.85	33.30	6.22	37.40	6.24
	C	893.51	15.95	863.24	29.63	802.61	41.45	860.88	32.58	788.71	66.60	711.82	67.30

Table 2 Statistics of (A) demineralized matrix thickness, (B) contact zone thickness and (C) mineralized matrix thickness measured in μm in acid-treated bone samples. Sample size equals 10 bones per group, except for anterior 0.5 M HCl containing 9 bones.

Region		2 hours						4 hours						Control	
		0.5 M HCl		1 M HCl		2 M HCl		0.5 M HCl		1 M HCl		2 M HCl			
		Mean	±SD	Mean	±SD	Mean	±SD	Mean	±SD	Mean	±SD	Mean	±SD	Mean	±SD
Anterior	A	1.57	0.026	1.58	0.029	1.56	0.032	1.57	0.030	1.55	0.033	1.53*	0.041	1.58	0.026
	B	1.44*	0.042	1.43*	0.044	1.44*	0.038	1.44*	0.031	1.41*	0.023	1.42*	0.062		
Posterior	A	1.60	0.046	1.59	0.031	1.58	0.039	1.59	0.036	1.58	0.021	1.58	0.045	1.59	0.020
	B	1.50	0.084	1.43*	0.032	1.49	0.046	1.45*	0.034	1.43*	0.111	1.50	0.067		
Medial	A	1.56	0.020	1.56	0.023	1.56	0.029	1.58	0.020	1.57	0.016	1.58	0.039	1.57	0.021
	B	1.47	0.032	1.45*	0.068	1.48	0.058	1.50	0.087	1.40*	0.086	1.40*	0.182		
Lateral	A	1.58	0.024	1.58	0.033	1.58	0.017	1.59	0.024	1.59	0.036	1.58	0.027	1.58	0.017
	B	1.40*	0.012	1.40*	0.020	1.42*	0.043	1.40*	0.019	1.41*	0.046	1.41*	0.065		

Table 3 Statistics of Ca:P in (A) mineralized matrix of acid-treated and control bones, (B) contact zone of acid-treated bones. Sample size equals 10 bones per group, except for anterior 0.5 M HCl containing 9 bones. *Acid-treated subsamples significantly different from controls within the corresponding anatomical region.

Acid Treatment	Anatomical Region	Ca:P
1 M/4 h	Posterior	0.96
2 M/4 h	Medial	1.11
2 M/4 h	Medial	1.01
2 M/4 h	Medial	1.04

Table 4 The Ca:P ratio in crystals from the contact zone of acid-treated bones.

		2 hours								4 hours							
		0.5 M HCl			1 M HCl			2 M HCl			0.5 M HCl			1 M HCl			2 M HCl	
Region		N	Mean	±SD	N	Mean	±SD	N	Mean	±SD	N	Mean	±SD	N	Mean	±SD	N	Mean	±SD
Anterior	A	0	0	0	10	45.443	44.347	10	92.738	76.631	9	9.109	16.255	10	56.821	77.385	9	91.879	50.496
	B	0	0	0	8	3.788	4.125	10	5.690	5.740	3	1.426	1.608	9	7.894	8.816	10	71.188	53.276
Posterior	A	10	9.795	22.941	10	56.074	64.960	10	121.634	63.504	10	17.137	20.216	10	64.925	50.748	10	97.535	48.811
	B	2	0.325	0.206	9	3.788	4.125	10	12.543	9.609	7	1.803	2.112	10	12.080	17.752	10	39.474	24.395
Medial	A	10	16.129	34.843	10	174.288	83.202	10	217.277	71.281	10	50.108	31.488	10	147.673	67.516	9	173.182	48.584
	B	2	0.892	0.238	10	14.829	8.266	10	52.076	28.744	10	5.520	4.804	10	36.993	18.540	10	87.722	44.437
Lateral	A	10	7.143	22.588	10	37.585	28.917	10	154.693	76.119	10	19.120	18.638	10	70.707	34.282	10	126.215	53.969
	B	1	0.860	0	8	2.88	2.516	11	11.0	8.967	6	1.64	1.601	11	16.6	16.57	11	34.5	25.5

6	9	0	25	6	0	31	4	0	75	79

Table 5 Statistics of (A) crystal number and (B) crystal area per 1 mm^2 of contact zone in acid-treated samples (mm^2 ×1000).